

Closure Report
(2019-22)

“Effect of energetic γ -photons and ion beams on the structural, opto-electronic and rheological property of tungsten dichalcogenides-based composites”

(UGC-DAE-CSR-KC/CRS/19/RC16/0987)

Submitted by

Principal Investigator

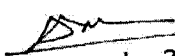
Prof. Dambarudhar Mohanta

Email: best@tezu.ernet.in

Department of Physics,

Tezpur University

PO: Napaam, Tezpur-784028, Assam


31-Oct-22

Principal Investigator
UGC-DAE-CSR Project
Department of Physics
Tezpur University

Project Fellow: Ms. Bhupali Deka, Department of Physics, Tezpur University

B. Deka.
31/10/22

Project summary

Abstract: At first, the liquid phase-based exfoliation (LPE) method was opted for based on co-solvent strategy. The dispersants, or solvents like NMP, DMF, etc. have been considered for exfoliation of as-purchased bulk WS₂ to nanoflakes. In addition, fractal-like patterns were grown by synthesizing exfoliated WS₂ nanoflakes onto sodium carboxymethyl cellulose (NaCMC) with varying concentrations using the solution mixing-evaporation technique. Moreover, radiation-induced effects through energetic particles or He²⁺ ion beam irradiation were studied on the layered WS₂ nanosheets. The WS₂ system exposed to UV- & β -rays showed enrichment in porosity leading to augmented photocatalytic activity. Furthermore, the He²⁺ ion irradiation has led to the exfoliation of the layered system in addition to surface patterning.

Key-words: TMD; exfoliation; nanoscale; irradiation; optical; photoactivity

1. Introduction and background

The inorganic, 2D transition metal dichalcogenide (TMDs) layered semiconducting WS₂ system consists of three atomic planes, with a typical 6-7 Å thick layers of chalcogen (S) atoms sandwiched between a hexagonally packed layer of metal (W) atoms. In its bulk or multilayer form, the indirect bandgap of WS₂ ranges between 1.3 and 1.4 eV, whereas in its bilayer and monolayer forms, the direct bandgap falls between 1.8 and 2.1 eV [1]. It was known that though the basal plane is very inactive, the edge sites, with their surface-active sites, are crucial for the catalytic application of TMDs. The 2D TMDs have significance in tunable optical, optoelectronic, electrical, electrochemical, and electromechanical characteristics. And their response to selective chemical and biosensing is also very encouraging depending on the number of layers, the chemical composition, the quantity of transition metal *d*-electrons. Additionally, point defects such as chalcogen vacancies in the systems show semiconducting, half-metallic, or metallic characteristics reported in earlier works [2].

In the realm of condensed matter research, pattern development in nano- or micro-structures resulting from the crystal growth of different polymer-containing composites or polymeric blends is also a topic of significant interest [3]. Witten and Sander, in 1981 formed a model, namely the diffusion-limited aggregation (DLA) model [4], which serves as the basis for the irreversible self-assembly development of complicated forms resulting in dendritic growth made up of numerous microscopic particles. The main factors responsible for pattern formation include particle transport phenomena, diffusivity, growth kinetics, anisotropic effect, supercooling, etc. A polysaccharide, namely sodium carboxy methyl cellulose (NaCMC) made up of the cellulose derivative (water-soluble) with carboxy methyl groups (-CH₂-COOH) linked to the part of monomers (hydroxyl group) comprised of glucopyranose. Due to the aforementioned ability to form films, hydrophilicity, low toxicity, and non-allergenic property, NaCMC has been recommended as a host, or cohost [5].

The layered 2D materials are thought to facilitate exceptional chemical and physical properties because of their hierarchical structural and morphological advantages over their bulk counterparts. The hierarchical porous materials contain the appearance of diverse ranges of porosity with variable sizes and length scales, including (i) micropores of dia. ~2 nm), (ii) mesopores of dia. in the range of ~2-50 nm), and (iii) macropores of dia. > 50 nm) [6]. In addition, a number of the pore size ranges described may have bimodal distributions as well as trimodal distributions. In particular applications with desired

functions, the existence of multiple ranges of changeable pores in a material system is significant [7]. Due to an increase in surface area, which facilitates electron transfer and increased photocatalytic activity, such micro-porous systems were thought to utilize light rather effectively [8].

To alter and manifest the physical characteristics of materials, ionizing radiation (e.g., gamma-rays), focused ion beams (FIB), and swift heavy energetic ions are often employed. Due to the strong interaction between the incident ions and the target material, modification to crystal structures, geometries, patterns, and chemical compositions can be realized for both bulk and nanosystems [9]. The primary way by which an energetic particle (ion, or electron) penetrates a solid or target medium and transfers its energy to the target atoms is a collision between the electrons of the target atoms. In general, as the ion beam travels through a solid target, the energy loss mechanism occurs via two processes: nuclear energy loss (S_n) and electronic energy loss (S_e). In general, when using a low-energy ion beam irradiation technique (i.e., up to a few tens keV regimes), nuclear energy loss is mostly carried on by elastic collisions that cause collision cascades that displace the atoms from their starting positions [10]. Furthermore, the nature of target material as well as ion beam energy, size and mass of the projectiles also serve as the crucial factors in determining the properties of post-irradiated samples.

Through this project work, the layered sheets of WS_2 that were processed via the LPE routes are exploited in detail along with radiation induced effects. To begin with, the creation of fractal-like structures has been realized after dispersing them in NaCMC. Moreover, the effects of radiation by ultraviolet (UV), beta (β), and gamma (γ) rays were also studied for the WS_2 nanosystems. In addition, the bombardment of low energy ion beams such as 15 keV He^{2+} onto the WS_2 system was characterized at varied fluences. The structural analysis, morphology, surface topology, composition, Raman signature, and vibrational modes of the pristine, composites and irradiated WS_2 nanosystems are discussed.

2. Objectives

- To analyze exfoliated, fractal structures and surface roughness of WS_2 /NaCMC composite films along with spectroscopic features.
- To study the adsorption-desorption isotherms, porosity measurements, spectroscopic analysis, and its photocatalytic activity in bulk form, exfoliated sheets, β -, and UV- irradiation effects on WS_2 sheets.
- To study the γ -irradiated structural, spectroscopic, and optoelectronic properties on exfoliated WS_2 systems with varying doses.
- Study of He^{2+} ion irradiation-induced effects on the WS_2 system with the formation and collapsing of helium bubbles.

2. Experimental: Materials and methods

2.1 Exfoliation of WS_2 sheets

Propan-2-ol (IPA, isopropanol, extrapure, FINAR® chemicals) and analytical grade tungsten disulfide (99% pure, WS_2 , grain size of 2 μm , Sigma Aldrich®) were obtained from various sources/agencies and utilized without additional purification steps. We attempted to exfoliate the purchased WS_2 powder in bulk form by dissolving it in water/IPA co-solvent. The bulk WS_2 of 0.32 g that we measured was put in 30 % IPA solvent. Now, the mixture was stirred for around 20 minutes using a magnetic stirrer to produce a uniform mixture for WS_2 . After further stirring, the mixture was exposed to ultrasonic waves in a sonicator (RoHS®, 100 W, 50 Hz) consistently for ~5 h and at an interval of 30 min. The precursors, which were produced after several hours of ultrasonication, were centrifuged at 2500 RPM for ~10 min. for WS_2 and the residue was then rinsed with DI (deionized) water several times. The precipitate was

allowed to get dry in an oven (hot air, REMI®) at a temperature of 70°C which comprises exfoliated sheets of WS₂.

2.2 Synthesizing WS₂/NaCMC based composite films

Sodium carboxy methyl cellulose sodium (NaCMC), obtained from Loba Chemie® was utilized without additional purification. A simple solution mixing-cum evaporation technique was used to produce WS₂/NaCMC composites. To begin, a 1% NaCMC solution was prepared by mixing 0.5 g of NaCMC in 50 mL of DI water. The NaCMC was magnetically stirred (1000 RPM) for at least one hour while maintaining a temperature of 70° for a homogeneous sol. Then, the exfoliated WS₂ (0.005 g) was added to the NaCMC sol and stirred at ~1000 RPM at a temperature of 60° for around 24 h with a pH ~7 to synthesize a 1 wt.% WS₂/NaCMC composite. Additionally, NaCMC (1.5 g) was dispersed in 150 mL of DI (deionized) water while being stirred at 1000 rpm for about an hour. Next, 0.015 g of exfoliated WS₂ was added, and stirring was maintained for another 48 h. In a similar way, 2-4 wt.% WS₂/NaCMC composites were also made. In order to prepare uniform films, the sol. was drop casted onto several microscopic slides. The films were then left to dry in an oven (hot air, REMI®) at a temperature of 70°C and further used for analysis purposes.

2.3 Effects of UV and β-particles on WS₂ systems

The exfoliated WS₂ sheets of 1.5 g (powder form) kept in a boat is brought under the UV cabinet for 30 min. kept 12 cm away from the UV lamp source (λ_{ex} = 365 nm). On the other hand, 1.5 g WS₂ is exposed to β-particles inside a Pb-shielded chamber (using a laboratory-grade-¹³⁷Cs as the source, offering energy ~1.17 MeV stable state), with a radioactivity of about 0.2 kGy in 30 min. All of the samples were handled at room temperature (300 K) and further examined for porosity study with regard to the impact of energetic particles on the system as well as in the bulk form that was bought directly and its exfoliated case.

2.4 Exposure of γ-photons on WS₂ systems

The exfoliated WS₂ was kept in a γ-irradiation chamber accessible at UGC-DAE CSR, Kolkata (source: ⁶⁰Co, dose rate=1.75 kGy/h, energy ~1.3 MeV,) at a temperature of 300 K. The specimens were irradiated for 0 kGy (pristine), 10 kGy, 25 kGy, 30 kGy, 35 kGy, and 40 kGy consequently, and categorized such as G0, G1, G2, G3, G4, and G5 for WS₂. The specimens after being exposed over stipulated time duration were taken out from the chamber after the requisite γ-doses.

2.5 Exposure of He²⁺ ions to WS₂ system

The bulk WS₂ purchased in powder form (with micron size) was directly infused over a teflon-pellet prepared from multipurpose teflon tape being crumpled into a thick circular disc of typical diameter ~13 mm. The WS₂ pellets were prepared by hot pressing onto the teflon support by a hydraulic press by applying a pressure of ~60 bar. The prepared specimens were exposed to low energy He²⁺ ion irradiation employing K130 variable energy cyclotron with the electron cyclotron resonance (ECR) ion source (6.4 GHz) available at Variable Energy Cyclotron Centre (VECC), Kolkata. The specimens were irradiated with fluences for 1×10¹⁵ ions/cm², 5×10¹⁵ ions/cm², 1×10¹⁶ ions/cm² and also irradiated at 55° angle for a particular fluence of 5×10¹⁵ ions/cm². The beam current was also checked during the experiment through the Faraday cup which was calculated to be around ~ 1.5 μA at 300 K and, the operating voltage was set at 7.5 kV giving a charge state of +2.

2.5 Characterization techniques

With the help of a field emission scanning electron microscope (FE-SEM, model: Zeiss, Sigma®) and attached energy dispersive spectroscopy (EDS) unit, the dried films casted over glass substrates were studied. AFM, NTEGRA Prima®, was utilized to examine the surface topography of the films. μ -Raman spectroscopy (EZRaman-N®), which has a laser operating at $\lambda=785$ nm and power 350 mW, was used to analyze the Raman spectra of the dried films. Also, Raman spectroscopy (Renishaw, UK), which uses an Ar⁺ ion laser excitation source operating at $\lambda=514$ nm and power 50 mW, was used to characterize WS₂ nanosystems exposed to radiation. The Fourier transform infrared (FT-IR) spectra were studied for dried films using a spectrophotometer (Nicolet Impact I-410®). Moreover, the N₂ adsorption-desorption isotherms and pore-size distribution using the NOVA 1000e® Quanta chrome system was used to characterize WS₂ irradiated to energetic particles. An X-ray diffractometer (D8 FOCUS, BRUKER AXS, Germany) attached with CuK α ($\lambda=1.54$) line source was used to ascertain the crystallinity and phase structure of WS₂. X-ray photoelectron spectroscopy (XPS) surface analysis was carried out using the PHI Versa Probe III model to examine the chemical state information of the material under study. Using a UV-Vis spectrophotometer (Lambda 365, PerkinElmer®), the absorbance of the samples as prepared was evaluated. Every experiment was carried out at room temperature (300 K).

3. Results and discussion

3.1 Study on the morphology and vibrational study of fractal patterns

Fig. 1(a,h) represents the FE-SEM images for 1-4 wt.% WS₂/NaCMC composites. In the case of a 1 wt.% sol. synthesized for 48 h, we see the emergence of longitudinal flat patterns that are oriented in one direction. However, a 1 wt.% sol. obtained in 24 h, reveals self-aggregate arrangements developed with fragments of irregular phases, caused by the addition of NaCMC in between the WS₂ layers through constant stirring, as shown in Fig. 1(b,f). On the contrary, the fractal patterns formed in the 2 and 4 wt.% may be due to the screening effect causing repulsion between the individual entities and is strongly influenced by the rate of diffusion. The patterns formed reasonably as a result of site-responsive percolation of NaCMC onto WS₂ by smearing away nanoflakes through diffusion-limited disruption (DLD) principle [11,12]. Fig. 1(i-l) represents the local fractal dimension (d_f) vs. frequency plots fitted with multi-peak Lorentzian functions showing the bimodal and trimodal distributions of self-similar fractal structures after deconvolution with asymmetrically broadened nature and having sharp maxima at $d_f = 2$ varying from 1.93 to 1.6 and indicating fractal-like patterns that have occurred in the layered WS₂ retaining its 2D nature as a background.

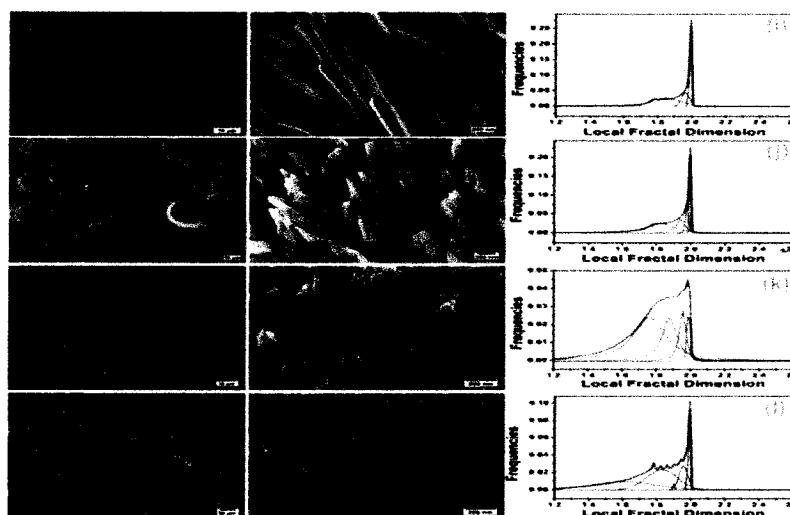


Figure 1: FE-SEM micrographs for (1-4 wt.%) composites of WS₂/NaCMC at (a-d) magnified at lower scale (scale bar: 10 μm), while (e-h) specify micrographs of higher magnifications (scale bar: 200 nm) of the specimens. The micrographs were taken for (a,e) 1 wt.% processed for 48 h, (b,f) 1 wt.% processed for 24 h, (c,g) 2 wt.% processed for 48 h, and (d,h) 4 wt.% processed for 48 h; (i-l) displays local fractal dimension (d_f) against frequency plots illustrated with Lorentzian fits for each system.

Fig. 2(a-f) displays the 2D surface scans and 3D topography of the films for 1-4 wt.% WS₂/NaCMC composites. The presence of fractal aggregates is also evident from the surface topography exhibiting self-similar pockets and oblates. Also, the calculated surface roughness parameter (σ) of the 1 wt.% case provides, $\sigma \sim 45.1$ nm while σ is moderately higher for 4 wt.% WS₂/NaCMC composite, i.e. $\sigma \sim 66.5$ nm. From the scanning analysis, various bumps are quite apparent through the multiple grains although the elongated structures seemed to have a smooth texture (Fig. 2(g-j)).

Fig. 3(a) displays the vibrational Raman spectra fitted with multi-peak Lorentzian functions of varying concentrations ranging from 16 wt.% to 1 wt.% of the WS₂/NaCMC nanocomposites. The two dominant first-order phonon optical modes, specifically, E'_{2g} in-plane mode and A_{1g} out-of-plane mode have appeared at ~ 350 cm⁻¹ and 418 cm⁻¹; respectively [13]. The E'_{2g}/A_{1g} mode intensity ratios of pure WS₂ (without NaCMC) together with 16 wt.% to 1 wt.% composite with increasing WS₂ content evaluated suggest a non-linear rising trend (Fig. 3(b,c)). Fig. 3(d) shows the FT-IR spectra of NaCMC, WS₂, and composites of WS₂/NaCMC for 1 wt.% to 16 wt.% respectively. The IR active molecules tend to get shifted and broadened due to the interaction among themselves, also the spectral fingerprints of both NaCMC and WS₂ have been retained in the composites.

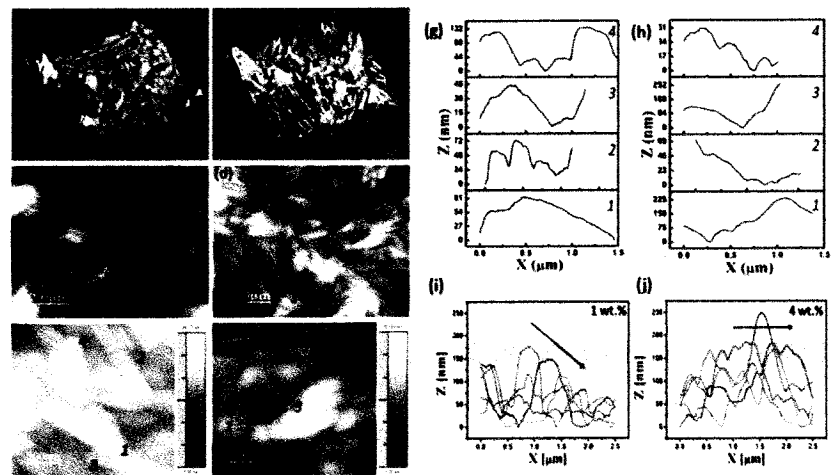


Figure 2: AFM of selected sites for 1 and 4 wt.% WS₂/NaCMC composites: (a,b) the 3D topography, (c,d) 2D surface scans, (e,f) 2D views (magnified) in a scale bar of 500 nm for directional scanning. The locations are designated by italicized numbers such as *1*, *2*, *3*, etc.; (g,h) directional height profiles for 1 & 4 wt.% WS₂/NaCMC composites, measured laterally along the designated lines. Here, (i,j) 5 specific locations were selected showing

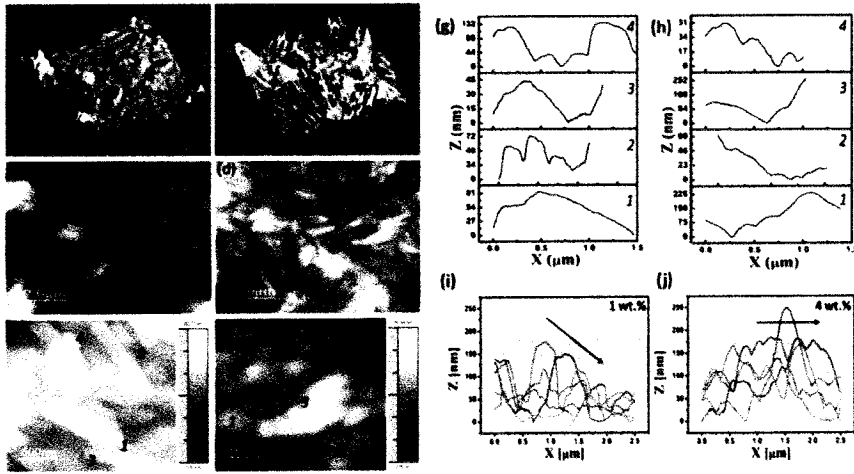


Figure 2: AFM of selected sites for 1 and 4 wt.% WS₂/NaCMC composites: (a,b) the 3D topography, (c,d) 2D surface scans, (e,f) 2D views (magnified) in a scale bar of 500 nm for directional scanning. The locations are designated by italicized numbers such as *1*, *2*, *3*, etc.; (g,h) directional height profiles for 1 & 4 wt.% WS₂/NaCMC composites, measured laterally along the designated lines. Here, (i,j) 5 specific locations were selected showing horizontal line scans for respective height profiles. Arrowhead lines from the left represent the specimen's variation in height over a range of distances.

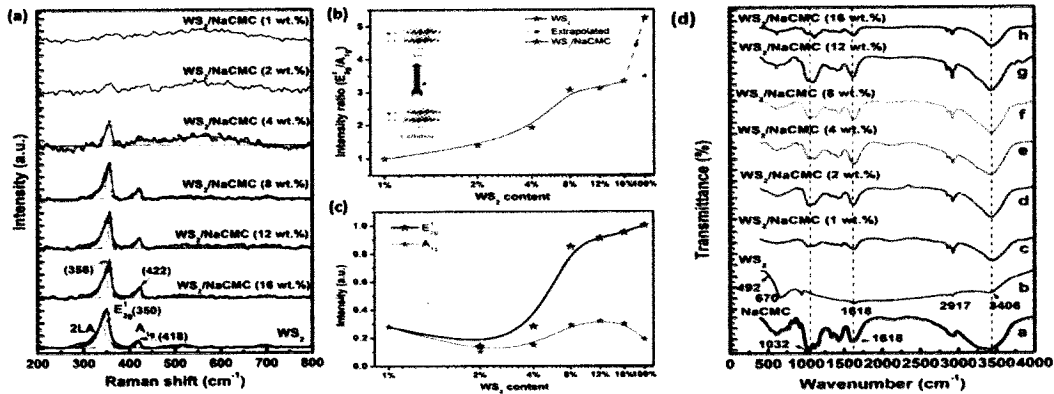


Figure 3: (a) Raman spectra shown for 1-16 wt.% composite systems of WS₂/NaCMC and of pure WS₂, (b) highlights the function of host matrix NaCMC in the pattern of intensity ratio ($E^{l_{2g}}$ -to- A_{1g}) mode for various loadings; (c) the intensities of $E^{l_{2g}}$ and A_{1g} modes exhibiting non-linear trend with increase in concentration of WS₂; (d) FT-IR spectra: NaCMC, WS₂, and 1 wt.% to 16 wt.% WS₂/NaCMC composites.

Table 1. Using the HRSEM analysis, fractal dimensions are determined through the local fractal dimension (f_d) vs. frequency plot, whilst the AFM study provides information on RMS roughness, skewness and kurtosis values.

Concentration (samples)	Fractal Dimension	RMS roughness (σ) (nm)	Skewness (S)	Kurtosis (K)
1 wt.% (24 h)	1.83 1.94 1.98	---	---	---
1 wt.% (48 h)	1.84 1.96	45.1 ± 6.02	-0.2024	5.8336
2 wt.% (48 h)	1.79 1.93 1.98	---	---	---
4 wt.% (48 h)	1.60 1.83 1.90 1.96	66.5 ± 15.03	0.5463	3.5675

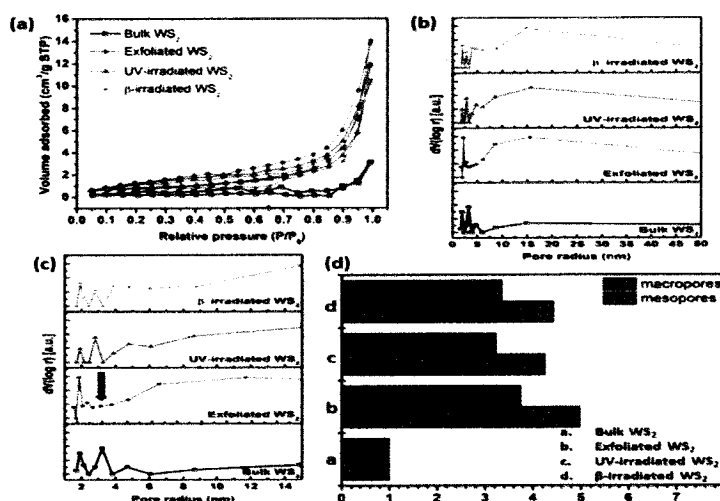


Figure 4: (a) N₂ adsorption-desorption isotherms, (b) the pore size distribution, (c) the distribution of pore sizes associated with bulk WS₂, exfoliated WS₂, irradiated with UV- and β -rays is shown in magnified view, respectively. (d) the area below the respective curves was compared within dia. ~ 8–100 nm, the meso- and macro-pore size distribution of the samples was calculated.

3.2 Effects of radiation (UV and β -rays) on porosity and its application in photocatalytic activities

Fig. 4(a),(b) illustrate, respectively, the isotherms and pore-size distribution of four distinct systems. Through the BJH model, the pore-size distribution was analyzed for bulk WS₂, exfoliated WS₂ nanosheets (NSs), and WS₂ exposed to UV rays ($\lambda_{\text{ex}} = 365$ nm for 30 min) and β -particles (0.2 kGy) examined through the Brunner-Emmett-Teller (BET) analysis by means of N₂ adsorption/desorption isotherms carried out at liquid nitrogen temperature (77 K). A typical type-IV curve showing the existence of meso-pores with dia. ~2-50 nm can be evident for a notable increase in volume adsorbed

in the range of relative pressure, $p/p_0 = 0.5-1.0$, as can be found in Fig.4(a). This is explained by the fact that capillary condensation takes place in mesopores that are quite big in size [14].

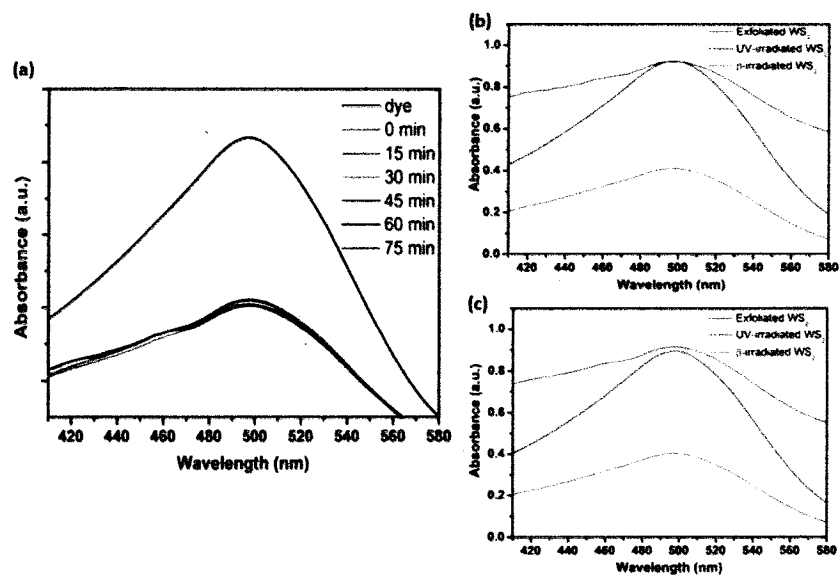


Figure 5. (a) WS₂ added Congo red (CR) dye absorbance spectra after exposures for upto ~75 min exposure; (b,c) a comparative plot for WS₂ (exfoliated), WS₂ exposed to UV- and β-rays for 15 and 45 minutes, respectively, as a catalyst added to Congo red dye.

The photocatalytic activity has been studied due to the presence of meso-macro pores in the WS₂ material witnessed from the BET analysis upon exposure with UV and β-rays. The UV-vis spectra displayed in Fig. 5 were used to analyse the efficiency of photocatalytic degradation exfoliated WS₂ and a comparative plot for exfoliated and exposed WS₂ systems on Congo red dye Fig. 5(a-c). The CR dye, which absorbs light in the blue region, has a strong absorbance peak maximum at around 497 nm with a broadened spectral nature. It has also revealed rapid degradation through the addition of WS₂ nanosheets as a catalyst irradiated for 75 minutes, leading to the cleavage of the dye molecule's -N=N bond. For up to 15 and 45 minutes, respectively, a relative plot for CR dye added with exfoliated WS₂, UV-, and β-irradiated WS₂ as a catalyst was also examined. Under UV light irradiation for 45 minutes, as indicated in Table 2, we could observe that the β-irradiated WS₂ system showed enhanced photocatalytic degradation of CR dye by efficiency of 59.38%. This could be because the WS₂ system has substantially more sulfur atomic vacancies than the WS₂ system that wasn't exposed to radiation, which is known to make it easier to transfer and separate photo-generated carriers and improve the performance of the catalyst in photocatalytic activity.

Table 2. Calculation of Congo red dye degradation percentage (%) using peak maxima of the absorbance spectra.

Sample	Degradation (%)	
	illumination for 15 min	illumination for 45 min
WS ₂ (exfoliated)	07.32	08.22
WS ₂ upon UV-irradiation	07.32	10.23
WS ₂ upon β -irradiation	58.55	59.38

3.3 Effects of He²⁺ ion irradiation on the WS₂ systems

When exposed to fluences of 1×10^{15} , 1×10^{16} ions/cm² for normal incidence and 5×10^{15} ions/cm² at a 55° incidence angle, as illustrated in Fig. 6, the hillocks present in pristine specimens begin to diminish their heights with the development of the corrugated surface texture (b,e,h,k). The RMS roughness determined by employing WSxM software version 5.0 (Nanotec, Inc.)[®] on the AFM micrographs reduced as compared to the bulk WS₂, although the amount is significantly dependent on the incidence cases (normal or oblique) and providing values ($r_{\sigma} \sim 0.36$ to 0.87 nm). The chemically inert He ions upon implantation, become charge neutral and diffusing to locally form nuclei within the projectile's range. As a result, bubble formation that weakens van der Waal forces leads to exfoliation and patterned surfaces [15]. Additionally, the systems under investigation subjected to ion irradiation result in defects formation such as vacancies or interstitials

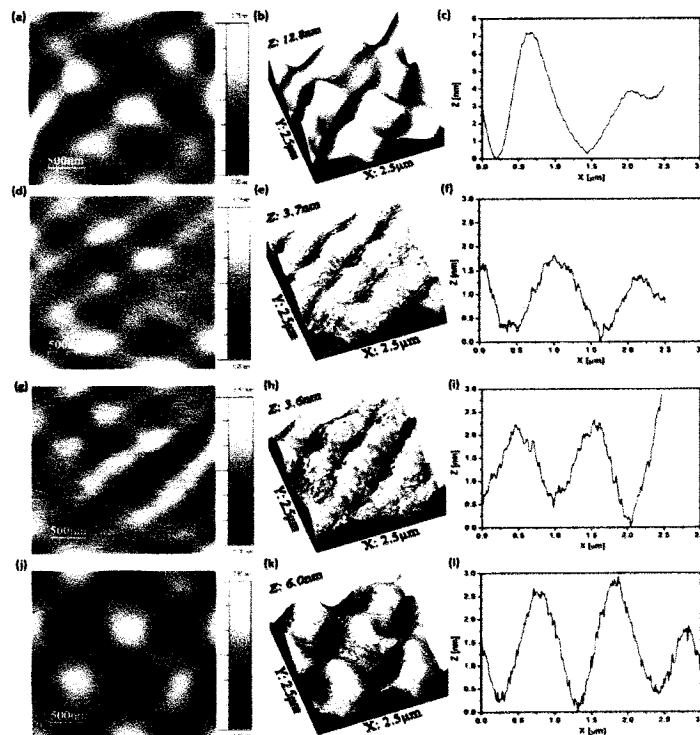


Figure 6. 2D surface scans (AFM images) of (a) pristine (bulk WS₂) and irradiated WS₂ for (d) 1×10^{15} ions/cm² at 0° normal incidence, (g) 5×10^{15} ions/cm² at 55° incident angle, and (j); 1×10^{16} ions/cm² at 0° normal incidence; (b,e,h,k) respective 3D topography images; (c,f,i,l) corresponding height profiles.

Fig. 7 shows the High-resolution transmission electron microscopy (HRTEM) images to analyse the morphology of the pristine (WS₂) and after irradiation with 15 keV He²⁺ ions for fluence 5×10^{15} ions/cm² at 0° and 55° incident angle; respectively. The edge angle (120°) showing the hexagonal structure of the WS₂ sheets can be seen in Fig. 7(a). Moreover, as a result of the creation of bubbles and the collapse of He nuclei between the Vander Waal bonded layers bombarded through He ions in the WS₂, the irradiated systems caused exfoliation by causing layers to separate from stacks seen in the pristine case (Fig. (c-f)). The irradiated system with a normal angle (0°) incident angle shows two sets of diffraction points in the corresponding selective area electron diffraction (SAED) shown as an inset (Fig. (e)). However, in the case of the 55° incident angle (Fig. (f)), only one set of distinct diffraction spots is seen strongly indicating the single crystallinity of layered WS₂ nanosheets.

Employing XPS analyses, Fig. 8(a-f) illustrates the chemical compositions and elemental states of the pristine and irradiated WS₂ for fluence 5×10^{15} ions/cm². The W4 f_{7/2} and W4 f_{5/2} states of tungsten are revealed in the deconvoluted XPS spectra produced using multi-peak Gaussian fitting as evidenced by two different peaks at 30.96 eV and 33.05 eV, respectively.

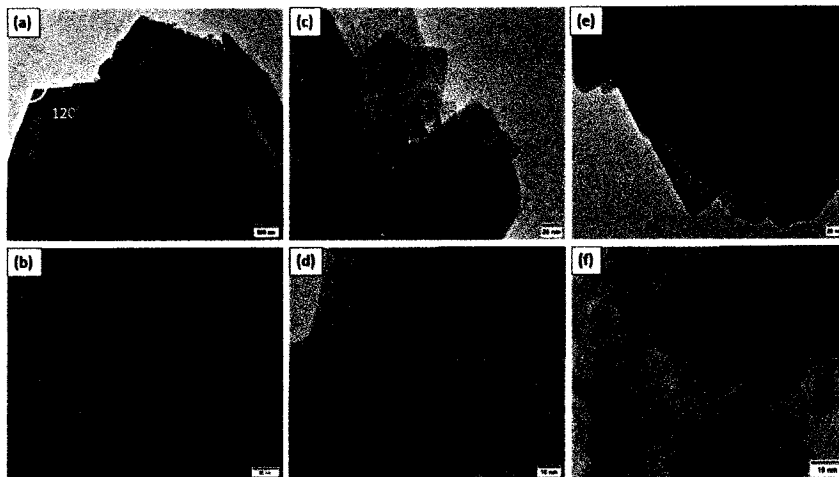


Figure 7. High-resolution transmission electron microscopy (HRTEM) images of (a,b) pristine (WS₂) case, after irradiation for fluence (c,d) 5×10^{15} ions/cm² at 0°; (e,f) 5×10^{15} ions/cm² at 55° incident angle respectively; note that SAED pattern of the irradiated WS₂ systems are shown as an inset (d,f).

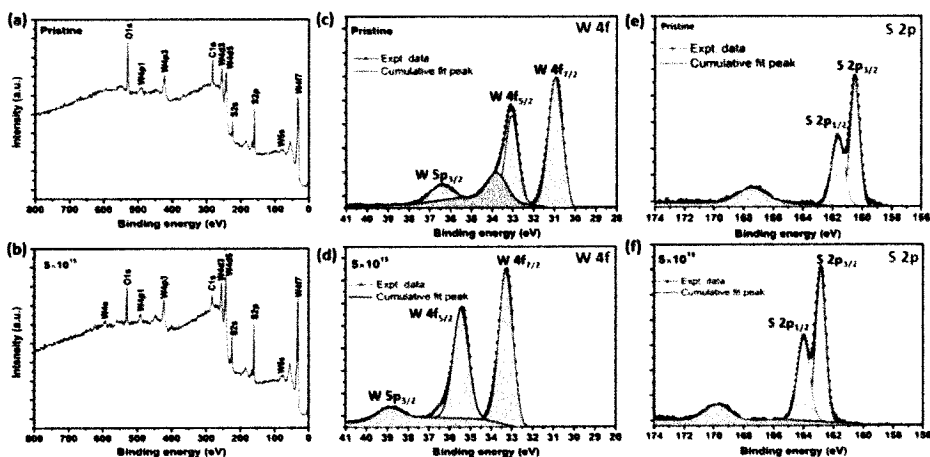


Figure 8. XPS survey scan: (a) pristine, (b) fluence (5×10^{15} ions/cm²) irradiated WS₂; (c) W4f-core level spectra (pristine case), (d) W4f-core level spectra (irradiated case); S 2p-core level of (e) pristine, and (f) irradiated WS₂.

These locations of the peaks are slightly shifted to ~ 33.29 eV and 35.47 eV; respectively and the W $5p_{3/2}$ state at ~ 38.90 eV (Fig. 8(c,d)) corresponds to the various binding energies that define the tungsten valence W^{4+} state [16]. In contrast to the pristine case, the peaks of the S element in the irradiated specimen moved toward greater binding energy situated at 162.85 eV and 164 eV, respectively ascribed to the S $2p_{3/2}$ and S $2p_{1/2}$ states of divalent sulfide ions (Fig. 8(e,f)) belonging to the phase-pure structure of WS₂.

References

1. S. Das, J.A. Robinson, M. Dubey, H. Terrones, M. Terrones, Beyond graphene: progress in novel two-dimensional materials and van der Waals solids, *Ann. Rev. Mat. Res.* **45** (2015) 1-27. <https://doi.org/10.1146/annurev-matsci-070214-021034>.
2. D. Jariwala, V.K. Sangwan, L.J. Lauhon, T.J. Marks, M.C. Hersam, Emerging Device Applications for Semiconducting Two-Dimensional Transition Metal Dichalcogenides, *ACS Nano* **8** (2014) 1102-1120. DOI: 10.1021/nn500064s.
3. D. Kaya, V.A. Belyi, M. Muthukumar, Pattern formation in drying droplets of polyelectrolyte and salt, *J. Chem. Phys.* **133** (2010) 114905. <https://doi.org/10.1063/1.3493687>.
4. T.A. Witten, L.M. Sander, Diffusion-Limited Aggregation, a Kinetic Critical Phenomenon, *Phys. Rev. Lett.* **47** (1981) 1400-1403. <https://doi.org/10.1103/PhysRevLett.47.1400>.
5. K. Thorkelsson, P. Bai, T. Xu, Self-Assembly and Applications of Anisotropic Nanomaterials: A Review, *Nano Today* **10** (2015) 48-66. <https://doi.org/10.1016/j.nantod.2014.12.005>.
6. M.H. Sun, S.Z. Huang, L.H. Chen, Y. Li, X.Y. Yang, Z.Y. Yuan, B.L. Su, Applications of hierarchically structured porous materials from energy storage and conversion, catalysis, photocatalysis, adsorption, separation, and sensing to biomedicine. *Chem. Soc. Rev* **45** (2016) 3479-3563. <https://doi.org/10.1039/C6CS00135A>.
7. M.G. Mohamed, E.C. Atayde, B.M. Matsagar, J. Na, Y. Yamauchi, K.C.W. Wu, S.W. Kuo, Construction Hierarchically Mesoporous/Microporous Materials Based on Block Copolymer and Covalent Organic Framework, *Journal of the Taiwan Institute of Chemical Engineers* **112** (2020) 180192. <https://doi.org/10.1016/j.jtice.2020.06.013>.
8. L. Su, L. Luo, H. Song, Z. Wu, W. Tu, Z.J. Wang, J. Ye, Hemispherical shell-thin lamellar WS₂ porous structures composited with CdS photocatalysts for enhanced H₂ evolution, *Chemical Engineering Journal* **388** (2020) 124346. <https://doi.org/10.1016/j.cej.2020.124346>.
9. S. Kretschmer, M. Maslov, S. Ghaderzadeh, M. Ghorbani-Asl, G. Hlawacek, A.V. Krasheninnikov, Supported Two-Dimensional Materials under Ion Irradiation: The Substrate Governs Defect Production, *ACS Appl. Mater. Interfaces* **10** (2018) 30827-30836. DOI:10.1021/acsami.8b08471
10. B. Schmidt, K. Wetzig, B. Schmidt, K. Wetzig, Ion Beams in Materials Processing and Analysis, Springer Vienna (2013). doi.org/10.1007/978-3-211-99356-9.
11. P.J. Yunker, M.A. Lohr, T. Still, A. Borodin, D.J. Durian, A.G. Yodh, Effects of Particle Shape on Growth Dynamics at Edges of Evaporating Drops of Colloidal Suspensions, *Phys. Rev. Lett.* **110** (2013) 1-5. DOI: 10.1103/PhysRevLett.110.035501.
12. R.M. D'Souza, N.H. Margolus, Thermodynamically reversible generalization of diffusion limited aggregation, *Phys. Rev. E* **60** (1999) 264-274.
13. H. J. Sarmah, D. Mohanta, A. Saha, Perceptible exciton-to-trion conversion and signature of defect mediated vibronic modes and spin relaxation in nanoscale WS₂ exposed to γ -rays, *Nanotechnology* **31** (2020) 285706. <https://doi.org/10.1088/1361-6528/ab7c4a>.
14. S.J. Hazarika, D. Mohanta, Exfoliated WS₂ nanosheets: optical, photocatalytic and nitrogen-adsorption/desorption characteristics, *Bull. Mater. Sci.* **41** (2018) 163. <https://doi.org/10.1007/s12034-018-1679-y>.
15. R. Hellborg, H.J. Whitlow, Y. Zhang, Ion Beams in Nanoscience and Technology, Springer Berlin, Heidelberg, (2010) 978-3-642-26137-4. <https://doi.org/10.1007/978-3-642-00623-4>.
16. X. Mao, Y. Xu, Q. Xue, W. Wang, D. Gao, Ferromagnetism in exfoliated tungsten disulfide nanosheets, *Nanoscale Research Letters* **8** (2013) 430.

5. Outcome/Publications (if any)

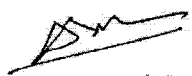
1. B. Deka, D. Mohanta, & A. Saha, Featuring exfoliated 2D stacks into fractal-like patterns in WS₂/carboxy methyl cellulose nanocomposites, *Surfaces and Interfaces*, **29** (2022) 101727. <https://doi.org/10.1016/j.surfin.2022.101727>

2. B. Deka & D. Mohanta, Altered mesopore distribution in exfoliated WS₂ nanosheets with radiation exposure, *Materialstoday: Proceedings*, **66** (7) (2022) 3405-3411.
<https://doi.org/10.1016/j.matpr.2022.07.317>.
3. B. Deka, D. Mohanta, & A. Saha, Controlling corrugated WS₂ surfaces upon bubbling with 15 keV He²⁺ ion irradiation, (*To be communicated*)

18. X. Mao, Y. Xu, Q. Xue, W. Wang, D. Gao, Ferromagnetism in exfoliated tungsten disulfide nanosheets, *Nanoscale Research Letters* 8 (2013) 430.

5. Outcome/Publications (if any)

1. B. Deka, D. Mohanta, & A. Saha, Featuring exfoliated 2D stacks into fractal-like patterns in WS₂/carboxy methyl cellulose nanocomposites, *Surfaces and Interfaces*, 29 (2022) 101727. <https://doi.org/10.1016/j.surfin.2022.101727>
2. B. Deka and D. Mohanta, Altered mesopore distribution in exfoliated WS₂ nanosheets with radiation exposure, *Materialstoday: Proceedings*, 66 (7) (2022) 3405-3411. <https://doi.org/10.1016/j.matpr.2022.07.317>.
3. B. Deka, D. Mohanta, and A. Saha, Controlling corrugated WS₂ surfaces upon bubbling with 15 keV He²⁺ ion irradiation, (To be communicated)


 Principal Investigator
 DST-SERB/CSCIR Project
 Department of Physics
 Tezpur University

B. Deka
 31/10/22
 (Project fellow)

FUND UTILIZATION CERTIFICATE

(2021-2022)

(Project/Schemes)

Name of Nodal Institute/Department of Organisation: TEZPUR UNIVERSITY (UGC-DAE-CSR KC/CRS/19/RC16/0426 dated 25-10-2021 & UGC-DAE,CSR/PROJECT/ACC/2022/0597 dated 21-01-2022)

Name of the Principal Investigator: Prof. Dambarudhar Mohanta

Funding Agency: UGC-DAE CSR, Kolkata Centre.

Certified that out of Rs. 45,000/- of grant-in aid on the 'Contingency & Consumables' and Rs. 1,81,440/- under the head 'Fellowship with HRA', the total grant of Rs. 2,26,440/- sanctioned to Registrar, Tezpur University received from the UGC-DAE CSR, KC under the scheme of support for project entitled "Effect of energetic γ -photons and ion beams on the structural, opto-electronic and rheological property of tungsten dichalcogenides-based composites" vide UGC-DAE CSR, KC letter No. UGC-DAE-CSR/PROJECT/ACC/2022/0597 dated 21.01.2022 towards the year 2021-2022, also from a balanced amount of Rs. 1,37,648/- from the year 2020-2021, the sum of Rs. 2,86,505/- has been utilized till 31st May 2022, for the purpose for which it was sanctioned and in accordance with the terms and conditions as laid down by the Commission. An amount of Rs. 4206/- was credited to the account from the bank as interest. The unspent balance till 31st May 2022 to be returned is Rs. 81,789/-.


Principal Investigator


(Prof. Dambarudhar Mohanta)

Principal Investigator
BSC-GERB/KC/CSR Project
Department of Physics
Tezpur University


Finance Officer

Finance Officer
Tezpur University
(Tezpur University)

For SURAJIT CHAKRABORTY & CO.
CHARTERED ACCOUNTANTS


CA. SURAJIT CHAKRABORTY
(Proprietor)
Membership No. - 305054

27/08/2022

STATEMENT OF EXPENDITURE

1. Name of the Principal Investigator : Prof. Dambarudhar Mohanta
2. Department of Principal Investigator : Dept. of Physics, Tezpur University
3. UGC-DAB CSR, KC approval Letter No. and Date : UGC-DAB-CSR
KC/CRS/19/RC16/0426, 25-10-2021.
4. Title of the Project: "Effect of energetic γ -photons and ion beams on the structural, opto-electronic and rheological property of tungsten dichalcogenides-based composites"
5. Effective date of starting the project : 1st June, 2019.
 - a. Period of Expenditure : From 1st June, 2021 to 31st May, 2022.
 - b. Details of Expenditure :

Sl. no	Heads of account	Received grant during 2019-2020 (₹)	Expenditure Incurred till 31 st May, 2020 (₹)	Received grant during 2020-2021 (₹)	Expenditure Incurred till 31 st May, 2021 (₹)	Received grant during 2021-2022 (₹)	Expenditure Incurred till 31 st May, 2022 (₹)	Balance (₹)
1.	Contingency	15,000	14,837	15,000	0	15,000	29,999	164
2.	Consumables	30,000	17,017	30,000	0	30,000	59,999	12,984
3.	Fellowship + HRA (8%)	1,68,000 + 13,440	1,17,058	1,68,000 + 13,440	1,66,320	1,68,000 + 13,440	1,96,507	64,435
4.	Interest on bank (P-III)							4,206
	Total	2,26,440	1,48,912	2,26,440	1,66,320	2,26,440	2,86,505	81,789

Unspent amount till 31st May, 2022 is Rs. 81,789/-. The unused amount should be returned through e-banking.

For SURAJIT CHAKRABORTY & CO.
CHARTERED ACCOUNTANTS

CA. SURAJIT CHAKRABORTY
(Proprietor)
Membership No. 305054

Dm
Principal Investigator
Principal Investigator
UGC-DAB-CSR Project
Department of Physics
Tezpur University

Dr. Surajit Chakraborty
Registrar
Registrar
Tezpur University

V. S. M.
Finance officer
Finance officer
Tezpur University